Calculation of the dynamics of gravity-induced density profiles near a liquid-vapor critical point

Hacène Boukari, Robert L. Pego, and Robert W. Gammon
Institute for Physical Science and Technology, University of Maryland, College Park, Maryland 20742
(Received 28 July 1994)

We develop one-dimensional equations that describe the dynamics of a highly compressible fluid in the presence of gravity. We apply these equations to a fluid near its liquid-vapor critical point and discuss how the coupling between gravity and compressibility affects the fluid bulk response to temperature changes. To illustrate the effect of this coupling on the equilibration process, we present numerical solutions for a one-phase critical fluid in the earth's gravity subjected to a sudden temperature step at the boundaries. We find that the adiabatic effect is responsible for accomplishing most of the temperature change in the fluid, within seconds, a rate far faster than that of thermal diffusion. On the other hand, the stratification of density under gravity takes hours, although this time is smaller than the diffusion time in the corresponding zero-gravity situation. Unlike the zero-gravity case, the adiabatic effect creates a small but significant temperature gradient immediately after the quench. As a consequence, diffusion in the fluid bulk begins earlier than it would otherwise. This gradient does not induce buoyant convective flow in the bulk, however, because of the fluid's compressibility. In the time range studied, no single exponential mode has emerged to dominate; a long intermediate regime spans a long period of time (many hours), which could lead to erroneous interpretation of experimental results.

PACS number(s): 44.10.+i, 66.10.Cb, 64.60.−i, 05.70.Jk

I. INTRODUCTION

Near the liquid-vapor critical point, a fluid becomes highly compressible and highly expandable: the coefficients of isothermal compressibility and isobaric thermal expansion both diverge strongly. This divergence plays a major role in the thermal equilibration of near-critical fluids. It has been shown that heat transfer into a near-critical fluid can occur rapidly via a mechanism that creates adiabatic pressure changes in the bulk of the fluid [1–7].

This adiabatic mechanism, usually neglected in ordinary incompressible fluids, can be briefly described as follows. If a temperature perturbation (such as a cooling step) is applied at the boundary of a fluid, it causes a contraction of the fluid near the boundary. As a result, in the interior of the fluid, the pressure drops uniformly and adiabatically and this causes the temperature to fall. Since the pressure changes are mediated by sound waves, the temperature change occurs much faster than could be accomplished by thermal diffusion acting alone.

This mechanism becomes particularly noticeable near the liquid-vapor critical point, as the fluid becomes highly expandable and compressible. In fact, we know now that, given the appropriate temperature changes at the boundary, the adiabatic mechanism dominates the early stages of thermal equilibration and even leads to a surprising critical speeding-up phenomenon [1,2,5]. This is to be contrasted with the well-known critical slowing down associated with thermal diffusion, occurring in the late stage of equilibration.

Using the adiabatic mechanism, it became possible to explain the puzzling short equilibration times of temperature observed in some early critical-point experiments [8,9]. More recently, several earth-bound and low-gravity experiments have unambiguously confirmed the presence of the mechanism [5–7,10] and have observed the critical speeding-up phenomenon [5].

Following these results, attention has shifted towards the equilibration of density variations in these fluids and the role of these variations in the interpretation of some measurements. While it is now established that the response time of the fluid temperature is fast compared to the diffusion time, the corresponding rate of density equilibration has not been well understood [11–13] and, in some instances, remains problematic. As an example, we take the results of recent C_v measurements performed by Straub and Nitsche [13] in microgravity. The investigators did not observe a strong enhancement of the C_v peak as expected and this behavior has been attributed to density variations in the fluid and their poorly understood relaxation times.

The problem of density equilibration is inherently very important for understanding earthbound experiments on critical fluids. Under gravity, a highly compressible critical fluid collapses under its own weight to form a large density gradient. This density stratification restricts the precision of measurements of fluid properties near the critical point [14]. Several authors have investigated both theoretically and experimentally the effect of the density gradient on the interpretation of measurements taken in an equilibrium state [14–16]. However, the dynamics of the density profile during equilibration have received little attention, mostly because the focus has been on the anomalous properties of the fluids, not on their hydrodynamics.

In an early paper, Gitterman and Steinberg [17] addressed the thermal equilibration of a critical fluid under gravity in terms of thermal diffusion only. They examined the effect of a gravity-induced density gradient on

the relaxation time in a one-dimensional diffusion equation. For a linear density gradient, Berg [18] recently gave an estimate of the gravity effects on the fluid dynamics and concluded that the final equilibration time constant is nearly the same in the presence or absence of gravity. Onuki and Ferrell [4] also estimated the effect of gravity on the dynamics and suggested a modification to the zero-gravity equations to include the gravitational field.

One may expect, however, that these results are not valid very close to the critical point. Indeed, the density profile becomes highly nonlinear, especially in the temperature range where the fluid properties are well characterized by their asymptotic behavior approaching the critical point [i.e., for $(T-T_c)/T_c < 10^{-4}$; see [14] and references therein]. Further, the analysis of these calculations do not take into account the effects of the early adiabatic responses on the late stage of equilibration dominated by diffusion. As will be shown below, it turns out that these effects are very important for understanding the overall equilibration. Finally, it is frequently suggested that convective flows must play a significant role in density equilibration since temperature gradients of the wrong sign can easily lead to a hydrodynamic instability of the stratified fluid. As we shall see, however, the adiabatic response makes it possible to avoid such instabilities.

Most experimental observations indicate that the time to form the gravity-induced density profile is undoubtedly rather long, on the order of hours to days [12]. As far as we know, the only reported measurement of the local density equilibration times appears to be the recent one of Zhong and Meyer [19–21]. Using a one-dimensional model, they also calculated effective relaxation times for a critical fluid under the presence of gravity and found good qualitative agreement with experiment. Such observations and calculations of long density equilibration times seem paradoxical in light of the fast equilibration times of temperature (measured in seconds) confirmed by recent investigations [5–7,10,13].

The purpose of this paper is to explain this difference by extending our previous zero-gravity study [2,22] to include the effects of gravity on heat transfer. Specifically, we shall derive a pair of equations appropriate to describe heat transfer and slow flow in a compressible, pure fluid, strongly affected by gravity, in a one-dimensional, slablike geometric configuration. These equations completely take into account one-dimensional fluid motions due to the effects of thermal expansion and gravitational compression, which can cause large density variations in the compressible fluids. Somewhat surprisingly, the equations are similar in form to those introduced in [2] for the corresponding zero-gravity case.

To illustrate the combined effects of the adiabatic mechanism and gravity, we shall present results from numerical solutions of our equations for a one-phase critical fluid responding to a temperature quench at the boundaries. In contrast to our earlier paper [2], where we concentrated on the early adiabatic regime, in the present work we have extended the numerical calculations much further in time, following some later stages of thermal relaxation together with the corresponding process of density stratification under gravity. In the numerical method, we allow all thermodynamic coefficients to vary as a function of time and space, accounting for all the nonlinearities due to the temperature and density variations through the equation of state.

We reserve a detailed discussion of the results for Sec. IV below. We can summarize the main points, however, as follows. First, we find that, under gravity, thermal diffusion becomes important at an earlier time than the corresponding time for the zero-gravity case [1–2,4]: a small but significant temperature gradient forms in the bulk rather quickly during the adiabatic process. This gradient causes the temperature to dip slightly *below* the final equilibrium temperature near the top of the fluid, reversing the direction of the heat flux at the top boundary.

Second, the process of diffusive equilibration is not well characterized by a single exponential decay time. No fundamental mode emerges to dominate the relaxation of the density variations, at least for many, many hours. Instead, a long transient regime is observed, intermediate between the regime dominated by the adiabatic mechanism and the expected diffusive regime dominated by a single exponentially decaying mode. This conclusion is consistent with the measurements and calculations of Zhong and Meyer [19–21]. Certain features of this intermediate regime remain unexplained, but the early adiabatic process appears to leave a long-lasting mark on the equilibration process.

Finally, it is natural to question whether it is reasonable to model the fluid motions as one dimensional. When cooling the fluid from the boundaries, it is easy to imagine that temperature gradients, especially near the top boundary, would tend to generate significant buoyancy-driven convective flows. However, we find, first, that the rapid adiabatic response makes it possible to avoid the creation of adverse temperature gradients near the top. Furthermore, the bulk of the fluid remains mechanically stable against convection, an effect essentially due to the compressibility of the fluid and the adiabatic nature of the initial response.

II. EQUATIONS FOR SLOW FLOWS WITH GRAVITY

Our starting point is the general hydrodynamic equations for a compressible fluid with heat conduction and gravity. We presume that the fluid is in local equilibrium, with an equation of state appropriate for conditions near the critical point (see Sec. III below). Energy dissipation through viscosity is neglected because its influence is small in the one-dimensional flows that we are considering. The material time derivative will be denoted by

$$\frac{D}{Dt}=\frac{\partial}{\partial t}+v\frac{\partial}{\partial z} . \tag{1}$$

The equations are as follows, expressing the conservation of mass, momentum, and energy [23]:

$$\frac{D\rho}{Dt}+\rho\frac{\partial u}{\partial z}=0 , \tag{2}$$

$$\rho\frac{Du}{Dt}+\frac{\partial P}{\partial z}=-\rho g\ , \tag{3}$$

$$\rho T\frac{Ds}{Dt}=\frac{\partial}{\partial z}\left[\lambda\frac{\partial T}{\partial z}\right]\ . \tag{4}$$

Here ρ is the density, u the velocity, P the pressure, T the temperature, s the entropy per unit mass, g the gravitational constant, and λ the thermal conductivity. The fluid is assumed to be contained in a slab of height (or thickness) L; we assume $0<z<L$.

It will be convenient to use the pressure and temperature as the fundamental thermodynamic variables. Thus, by expressing $s=s(T,P)$ and $\rho=\rho(T,P)$ through the equation of state, we rewrite, as in [2], the continuity and energy equations as

$$\kappa_T\frac{DP}{Dt}-\alpha_p\frac{DT}{Dt}+\frac{\partial u}{\partial z}=0\ , \tag{5}$$

$$\frac{DT}{Dt}-\left[1-\frac{c_v}{c_p}\right]\left[\frac{\partial T}{\partial P}\right]_\rho\frac{DP}{Dt}=\frac{1}{\rho c_p}\frac{\partial}{\partial z}\left[\lambda\frac{\partial T}{\partial z}\right]\ . \tag{6}$$

Here κ_T is the isothermal compressibility, α_p is the isobaric thermal expansion coefficient, and c_p and c_v are the specific heats at constant pressure and volume. These are defined by

$$\kappa_T=\frac{1}{\rho}\left[\frac{\partial\rho}{\partial P}\right]_T,\quad \alpha_p=-\frac{1}{\rho}\left[\frac{\partial\rho}{\partial T}\right]_P\ , \tag{7}$$

$$c_v=\frac{1}{T}\left[\frac{\partial s}{\partial T}\right]_\rho,\quad c_p=\frac{1}{T}\left[\frac{\partial s}{\partial T}\right]_P\ . \tag{8}$$

The system of equations (3), (5), and (6) can be used to study the influence of hydrodynamics on heat transfer, on a time scale appropriate for resolving sound waves (or shock waves). Here we are interested in dynamic behavior that occurs very slowly compared to the time it takes for sound waves to cross the cell. A systematic procedure for obtaining simplified equations for compressible flows on long time scales was introduced by Majda and Sethian [24] in the context of combustion theory. (See also [25] and [26].)

In Appendix A we apply this procedure. We nondimensionalize the equations and estimate the size of the various terms, taking parameters appropriate to a typical experiment of interest. We find that the acceleration term $\rho\partial u/\partial t$ in Eq. (3) has by far the smallest contribution, at least two orders of magnitude smaller than the rest of the terms. To obtain a simplified set of equations, therefore, we neglect this term. Besides the viscosity, we neglect *only* this term. The simplified momentum equation that results is a hydrostatic pressure equation

$$\frac{\partial P}{\partial z}=-\rho(z,t)g\ . \tag{9}$$

Integration yields

$$P(z,t)=P_a(t)-g\int_0^z\rho(h,t)dh\ . \tag{10}$$

Here $P_a(t)$ is the pressure at the bottom wall and the integral term represents the total weight of the fluid below the height z. By denoting the integral term in Eq. (10) by P_g, we can write the pressure as

$$P(z,t)=P_a(t)+P_g(z,t)\ , \tag{11}$$

which is similar to the equation suggested by Onuki and Ferrell [4].

We do not intend to neglect the effects of fluid velocity on density changes in Eqs. (5) and (6). However, at this point the determination of the velocity can be *entirely decoupled* from the determination of the pressure and temperature fields [25]. This is done by introducing the material coordinates defined by

$$z'=\int_0^z\rho(h,t)dh,\quad t'=t\ . \tag{12}$$

Let $M=\int_0^L\rho(h,t)dh=\langle\rho\rangle L$ be the total mass of fluid in the cell. ($\langle\rho\rangle$ is the average density in the cell.) The change of variables $(z,t)\to(z',t')$ means that derivatives change via

$$\frac{\partial}{\partial z}\to\rho\frac{\partial}{\partial z'},\quad \frac{D}{Dt}\to\frac{\partial}{\partial t'}\ , \tag{13}$$

where the boundary conditions $u(0,t)=u(L,t)=0$ are applied. The meaning of these formulas for changing variables may be stated as follows. Since z' denotes the total mass of fluid lying below height z at time t, keeping z' fixed means following a particular material layer of fluid in the cell. This means that the material derivative changes into the partial time derivative.

Using the new coordinates, the pressure in Eq. (10) may be expressed as the difference of a time-dependent term $P_a(t')$, the pressure at the bottom of the cell, and a time-independent term gz'. Then it follows that $\partial P/\partial t'=dP_a/dt'$. An equation for this quantity may be obtained by integrating Eq. (5) over the cell, using $u(0,t)=u(L,t)=0$. What results is the system of equations

$$P(z',t')=P_a(t')-gz'\ , \tag{14}$$

$$\frac{\partial T}{\partial t'}-\left[1-\frac{c_v}{c_p}\right]\left[\frac{\partial T}{\partial P}\right]_\rho\frac{dP_a}{dt'}=\frac{1}{c_p}\frac{\partial}{\partial z'}\left[\rho\lambda\frac{\partial T}{\partial z'}\right]\ , \tag{15}$$

$$\frac{dP_a}{dt'}=\frac{\int_0^M\frac{\alpha_p}{\rho}\frac{\partial T}{\partial t'}dz'}{\int_0^M\frac{\kappa_T}{\rho}dz'}\ . \tag{16}$$

Equation (16) expresses the conservation of total mass. Notice that both integrals in Eq. (16) are performed over the total linear mass $M=\langle\rho\rangle L$.

Equations (15) and (16) are coupled integro-differential equations that, along with Eq. (14), represent the basic equations studied in this work. In this system, the density ρ is determined from P and T through the use of the hydrostatic pressure equation (14) and the equation of state. Thereby, this system, Eqs. (14)–(16), describes the dynamics of the temperature and pressure fields in the fluid under gravity. Once these equations have been used to find T and P as functions of the material coordinates (z',t'), one can determine T and P as functions of height z and time t by computing

$$z(z',t')=\int_0^{z'}\frac{1}{\rho(h',t')}dh' \tag{17}$$

(T or P can be plotted vs z parametrically).

It is interesting to compare the system of equations (14)–(16) with the corresponding equations used in [2] for the zero-gravity case. The latter equations are

$$P(z,t)=P_a(t)\ , \tag{18}$$

$$\frac{\partial T}{\partial t}-\left[1-\frac{c_v}{c_p}\right]\left[\frac{\partial T}{\partial P}\right]_\rho\frac{dP_a}{dt}=\frac{1}{\rho c_p}\frac{\partial}{\partial z}\left[\lambda\frac{\partial T}{\partial z}\right]\ , \tag{19}$$

$$\frac{dP_a}{dt}=\frac{\int_0^L\alpha_p\frac{\partial T}{\partial t}dz}{\int_0^L\kappa_T dz}\ . \tag{20}$$

The new equations (14)–(16) are more general than Eqs. (18)–(20) since, in addition to the effect of gravity, the effects of motion on the density changes due to expansion and contraction are included. Only the inertial forces due to fluid acceleration are neglected in Eqs. (14)–(16).

Nevertheless, the functional forms of Eqs. (15) and (16) are strikingly similar to Eqs. (19) and (20) studied in [2] for zero gravity. Consequently, the numerical procedure used to solve them is little different from that used in [2,22]. More interestingly, the role of each term in the new equations can be interpreted in a manner similar to that in [2]. In particular, Eq. (16) describes the time-dependent pressure changes responsible for the fast, adiabatic temperature response in pure fluids near the critical point. The effect of gravity appears explicitly only in the hydrostatic equation (14). The new term $P_g=-gz'$ is what allows the formation of the nonuniform equilibrium density profile, through the use of the equation of state at the constant equilibrium temperature.

The adiabatic mechanism of heat transfer due to the presence of the pressure term in Eq. (15) remains effective in the presence of the gravitational field. As the critical point is approached, the divergence of c_p, on one hand, diminishes the influence of the right-hand side of Eq. (15), confining thermal diffusion to the region very near the fluid boundaries where the temperature gradient is large. On the other hand, $c_v/c_p\to 0$ and the adiabatic term on the left-hand side dominates the time dependence of temperature. Compared to the zero-gravity case studied in [2], the effect of the pressure term in Eq. (15) on the overall temperature dynamics in the fluid can be different because of the density variations caused by gravitational compression and thermal expansion or contraction.

III. NUMERICAL SOLUTION

In the following, we present numerical solutions of Eqs. (15) and (16) for a critical fluid subjected to a temperature step at the boundaries. Physically, this computation is meant to model a boundary temperature change that occurs gradually compared to the acoustic time scale but rapidly compared to the relaxation times of interest.

We chose xenon as a working fluid since its critical properties are known, including its equation of state. Near the critical point, several models have been proposed in the literature for the equation of state, which include the various scaling laws in a consistent way (see [14] and references therein). Here we use the "restricted cubic model" defined in terms of the parametric variables r and θ. In Table I we list the various thermodynamic functions as well as the values of the critical exponents applied in this work. For the thermal conductivity, we apply the approach explained in [27,28] to calculate the background term and the divergent part near the critical point. Moreover, for consistency, we take from Ref. [27] the expressions describing the transport coefficients as a function of temperature and density for xenon (although more recent measurements on fluid viscosity have been reported [29]).

The numerical method involves the finite-difference approximation of functions of the two variables z' and $t=t'$. The fluid's linear mass M is divided uniformly into N small segments, or "spatial" steps, of constant size $\delta z'=M/N$, N being an integer number. To ensure convergence, the spatial and temporal steps $\delta z'$ and δt must satisfy the condition $D_f\delta t/\delta z'^2<\frac{1}{2}$, a criterion derived for the thermal diffusion equation. Here $D_f=\rho\lambda/c_p$, where the values in this expression are calculated at the final temperature and the critical density. Also, we find that N must be kept large enough to ensure good resolution, especially near the boundary in the early, fast adiabatic regime. Typically, we take $N=400$ for the computations in this work. This number represents a reasonable compromise between computational cost and accuracy.

The computation proceeds stepwise according to the flowchart in Fig. 1. We start by calculating the initial density distribution at the chosen initial temperature T_i, using the expression given by Eq. (14) for the pressure and the equation of state (see Appendix B for details). For this purpose, we take z' in the interval $-M/2<z'<M/2$ and set $z'=0$ as the reference point corresponding to $P(\rho_c,T_i)$, T_i being the initial equilibrium temperature. [A corresponding change is made in the ranges of integration for the integrals in Eq. (16).]

After each time step, the new temperature distribution is computed. This is followed by the calculation of the new density distribution, calculated from the equation of state $P(z',t)=P[\rho(z',t),T(z',t)]$, expressed in (r,θ) space. Then, we take the old value of pressure P at point z' and the value of the temperature T newly calculated at the same location and determine the new value of the density. Appendix B gives the details of the numerical method applied to switch back and forth between (P,T) space and (r,θ) space. From the newly calculated density and temperature distributions, we evaluate the new values of the various thermodynamic coefficients at each spatial point. Then we determine the pressure change allowing the calculation of the new value of the time-dependent part of pressure $P_a(t)$. The process repeats: from the pressure change, we go back to the heat transport equation and advance the temperature. Notice that, with this approach, all the thermodynamic coefficients are allowed to vary spatially and in time.

To illustrate the results, we start with the example of a

TABLE I. Restricted cubic model equations used in the calculations. For details, see [14] and references therein.

Dimensionless units	$T^*=T/T_c$, $P^*=P/P_c$, $\rho^*=\rho/\rho_c$, $c_v^*=c_vT_c/\rho_cP_c$
Variables	$\Delta T^*=r(1-b^2\theta^2)$
	$\Delta\rho^*=r^\beta k\theta(1+c\theta^2)$
Symmetrized compressibility	$K_T^*=(k/a)r^{-\gamma}$
Pressure	$P^*=(1+5.92\Delta T^*)+r^{\beta\delta}a\theta(1-\theta^2)+r^{2-\alpha}ak[\theta^2(1-\theta^2)(1+c\theta^2)-f(\theta)]$
Pressure coefficient	$(\partial P^*/\partial T^*)_\rho=5.92+r^{1-\alpha}aks(\theta)+(1+\Delta\rho^*)r^{\beta\delta-1}a\beta\theta\{\delta(1-\theta^2)(1+3c\theta^2)-(1-\theta^2)(1-c\theta^2)\}/q(\theta)$
Heat capacity	$c_v^*/T^*=-14.83/T^*+r^{-\alpha}ak\{(1-\alpha)(1-3c\theta^2)s(\theta)-\beta(1+c\theta^2)\theta s'(\theta)\}/q(\theta)$
Correlation length	$\xi=r^{-\nu}\xi_0R(\theta)$
Auxiliary functions	$f(\theta)=-0.770+2.359\theta^2-1.660\theta^4-0.059\theta^6$
	$s(\theta)=1.456-2.274\theta^2-0.073\theta^4$
	$q(\theta)=1-0.281\theta^2-0.166\theta^4$
	$R(\theta)=1+0.16\theta^2$
Constants	$a=15.4$
	$b^2=1.2766$
	$k=0.89$
	$c=0.055$
Exponents	$\alpha=0.11$
	$\beta=0.325$
	$\gamma=1.24$
	$\nu=0.63$
	$\delta=4.85$
Critical values of xenon	$T_c=289.72$ K
	$P_c=5.84\times10^6$ Pa
	$\rho_c=1110$ kg/m^3
Amplitude of correlation length	$\xi_0=1.78\times10^{-10}$ m

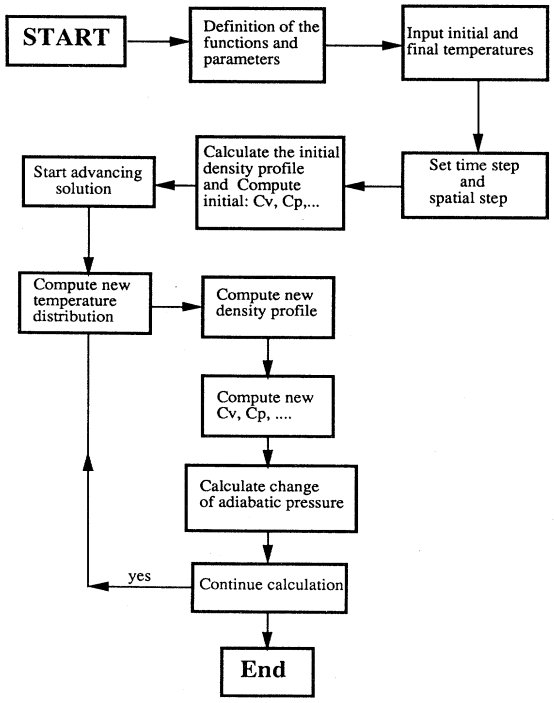

FIG. 1. Flowchart used to solve numerically Eqs. (14)–(16).

xenon sample whose boundaries are rapidly cooled from $T_i=T_c+20$ mK to $T_f=T_c+10$ mK. The fluid is initially in thermal equilibrium at T_i, with a fully developed density gradient. The fluid's total linear mass is taken to be $M=\rho_cL$, where $L=5$ mm. Because of the choice of the origin z', the actual thickness of the fluid slab is

$$L_*=\int_{-M/2}^{M/2}\frac{dz'}{\rho}\ .$$

This is extremely close to L because of the near symmetry of the density profile [see Fig. 3(a)] and so the average density $\langle\rho\rangle=M/L_*$ is very close to ρ_c. The fluid mass M is divided into 400 segments and the time step is $\delta t=0.05$ s.

We show in Fig. 2 the temperature profile in the first 60 s. While the effects of diffusion remain confined near the boundaries, the temperature in the bulk of the fluid has changed quickly due to the adiabatic effect. Compared to the corresponding zero-gravity case where the temperature change is uniform in the bulk (far from the boundary layer), a small, almost linear temperature gradient develops (but only in these early times). The gradient is *negative,* raising the concern that convective flows may be generated physically. Why this gradient forms and its relation to hydrodynamic stability will be discussed in some detail below.

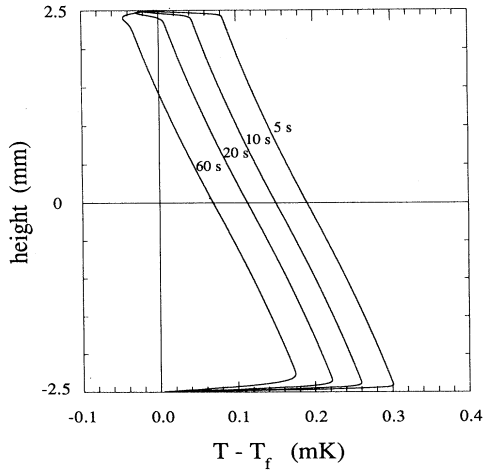

FIG. 2. Temperature profiles are shown along the height of a one-dimensional sample of xenon under gravity immediately following a temperature quench from $T_i - T_c = 20$ mK to $T_f - T_c = 10$ mK. Each profile is labeled by the time following the quench.

But notice also that the temperature locally near the top boundary has dropped *below* the final temperature. This surprising phenomenon is evidently due to the formation of the small temperature gradient, at the same time that the adiabatic mechanism is acting to lower the temperature at an almost uniform rate in the bulk. When the temperature near the top boundary arrives close to T_f or is slightly below, there remains a sharp temperature gradient at the bottom boundary, causing a further contraction of the fluid there and continuing to lower the pressure in the bulk via the adiabatic effect. It appears that this effect continues roughly until the temperature gradient near the top *reverses* sufficiently to create a balancing effect. Fluid will *expand* near the top boundary, with an effect on pressure changes opposing that of the contraction near the bottom. When the two effects achieve approximately equal strength, the adiabatic mechanism ceases to strongly affect the bulk of the fluid.

In Fig. 3(a) we show the dynamics of the density profile corresponding to the temperature profile shown in Fig. 2. While the temperature in the bulk has significantly approached its final temperature T_f within the first minute (close to 99% of the 10-mK step, Fig. 2), the change of density in the bulk is very small compared to the change needed to adjust to the final density profile. Thus the adiabatic mechanism has little effect on the density profile, as already explained by Onuki and Ferrell in [4].

Figures 3(b) and 3(c) show in detail the large density variations near the boundaries that are due to thermal diffusion. Because of the large thermal expansion coefficient of the critical fluid, the fluid at the boundaries experiences a significant change of density after the sudden temperature drop.

The large negative temperature gradient and dense boundary layer at the top suggest that some amount of convection may begin in the top boundary layer, al-

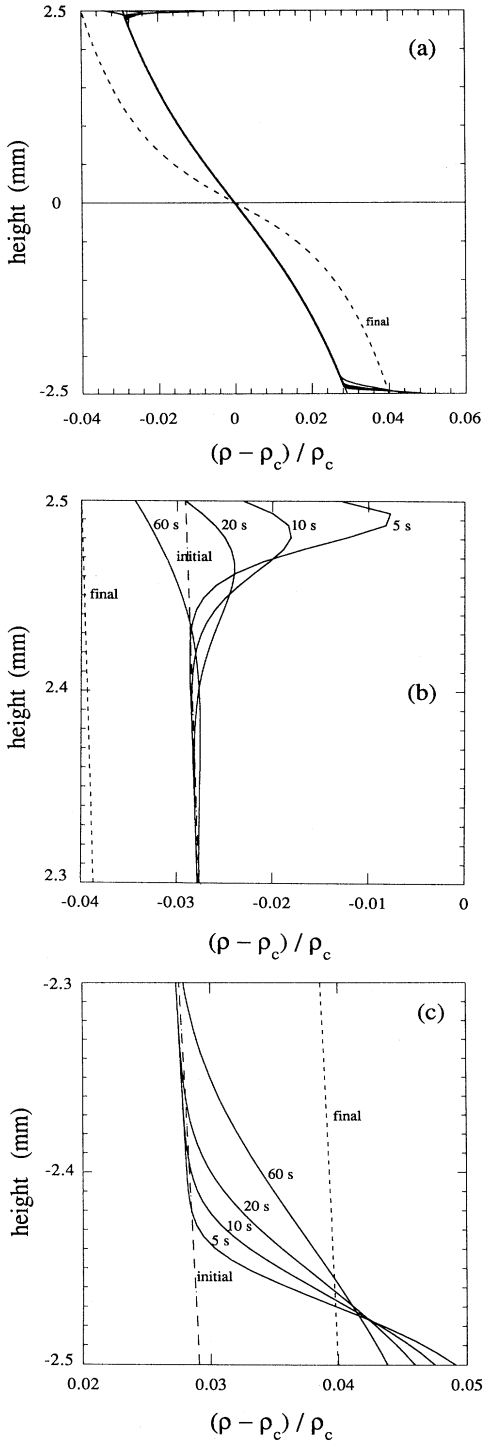

FIG. 3. (a) Density-profiles, in reduced units $(\rho - \rho_c)/\rho_c$, are shown along the height of a one-dimensional sample of xenon under gravity immediately following a temperature quench from $T_i - T_c = 20$ mK to $T_i - T_c = 10$ mK. (b) Details of the density changes as well as the initial and final density profiles are shown near the top boundary. The time in seconds following the quench labels each profile. (c) Details of the density changes as well as the initial and final density profiles are shown near the bottom boundary. The time in seconds following the quench labels each profile.

though it is possible that viscosity or dynamic processes might retard the development of such convection until the bulk temperature near the top wall is forced below the wall temperature by the adiabatic effect and a positive temperature gradient is established in the boundary layer. A multidimensional hydrodynamic stability analysis would appear to be necessary to assess the influence of convection during the initial stages of the quench.

Our analysis here will proceed under the assumption that the flow remains essentially one dimensional and that any convection in the top boundary layer has little influence on the later dynamics. We point out, however, that the sudden change of temperature that we have imposed here is an idealization of some more gradual adjustment of temperature on the boundary and it is relatively easy to alter the cooling procedure to completely avoid the creation of a negative temperature gradient in the top boundary layer. The bottom wall should be cooled first and the temperature at the top wall brought down at a rate designed to trail the behavior of the bulk temperature as determined by the adiabatic effect. In an experiment, such a delay could be achieved without requiring separate control of top and bottom temperatures by using materials of different heat conductivities for the top and bottom walls, for example, which respond at different rates to changes in bath temperature.

In Fig. 4 we plot computed temperature profiles corresponding to such a modified cooling procedure. In this computation, the temperature at the bottom wall is stepped from $T_i = T_c + 20$ mK to $T_f = T_c + 10$ mK suddenly, but the temperature at the top wall is decreased more gradually; the temperature as a function of time at the top wall is $T_f + (T_i - T_f)/(1+3t)$ mK. Due to the influence of the bottom boundary layer via the adiabatic effect, the temperature in the bulk near the top remains below that of the top boundary and the gradient in the top boundary layer remains positive throughout the computation. After 180 s, the temperature profile is very close to that obtained from the sudden quench as illustrated in Fig. 2. Profiles at much later times are indistinguishable. Corresponding density profiles in the top boundary layer are plotted in Fig. 5. Here we notice that unlike the dense, possibly unstable layer seen in Fig. 3(b) for a sudden quench, the gradual temperature change at the top boundary is helpful in avoiding the appearance of such a layer. (Note that in the absence of the adiabatic effect, in order to avoid negative temperature gradients at the top, the top wall temperature would have to be decreased much more slowly, on the time scales of hours associated with heat diffusion.)

The appearance of the temperature gradient in the bulk very early in the equilibration can be attributed to the adiabatic effect and explained by the presence of the gravitational field and the sensitive dependence of c_p on temperature near the critical point. We may understand this as follows. Taken with respect to material coordinates, the pressure gradient and temperature gradient are always related to the entropy gradient via

$$\frac{\partial s}{\partial z'} = \left[\frac{\partial s}{\partial T}\right]_P \frac{\partial T}{\partial z'} + \left[\frac{\partial s}{\partial P}\right]_T \frac{\partial P}{\partial z'} = \frac{c_p}{T}\frac{\partial T}{\partial z'} - \frac{c_p - c_v}{T}\left[\frac{\partial T}{\partial P}\right]_\rho \frac{\partial P}{\partial z'} . \tag{21}$$

In the initial equilibrium state, temperature is constant, so $\partial T/\partial z' = 0$. From Eq. (14), the pressure gradient is always given by $\partial P/\partial z' = -g$. As long as the processes in the bulk proceed adiabatically, the entropy gradient and

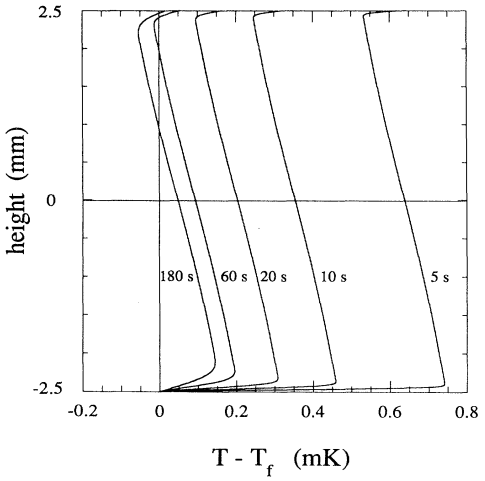

FIG. 4. Temperature profiles are shown along the height of a one-dimensional sample of xenon under gravity immediately following a sudden temperature quench at the bottom wall and a gradual decrease of temperature at the top wall of functional form $T_f + (T_i - T_f)/(1+3t)$. The initial and final temperatures are $T_i - T_c = 20$ mK and $T_f - T_c = 10$ mK, respectively. Each profile is labeled by the time in seconds following the temperature quench at the bottom wall.

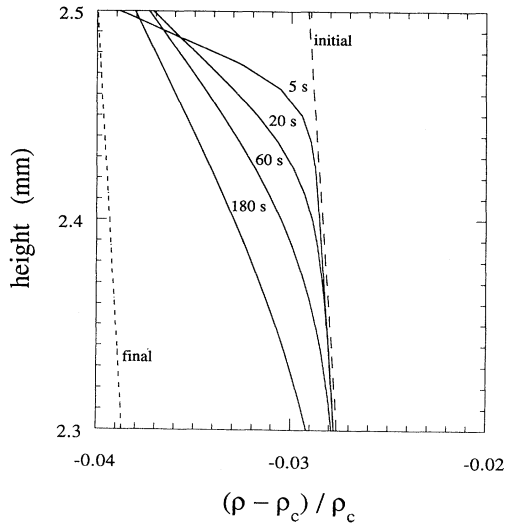

FIG. 5. Details of the density changes as well as the initial and final density profiles near the top boundary corresponding to the temperature profiles of Fig. 4.

pressure gradient will remain the same. As the values of temperature and pressure change, however, the coefficient $(\partial s/\partial P)_T$ in Eq. (21) will change and it is this change that creates the temperature gradient.

We may estimate the magnitude of this temperature gradient generated by the adiabatic mechanism as follows. We shall apply the superscripts (i) and (a) to quantities corresponding, respectively, to the initial time and a time after the adiabatic mechanism has largely equilibrated the temperature near the final value T_f (see Fig. 2). According to the above considerations and Eq. (21), we find that

$$\frac{c_p^{(a)}}{T^{(a)}}\frac{\partial T^{(a)}}{\partial z'}-g\left[\frac{\partial s}{\partial P}\right]_T^{(a)}=-g\left[\frac{\partial s}{\partial P}\right]_T^{(i)}. \tag{22}$$

To obtain an approximation for the magnitude of the resulting temperature gradient, it suffices to observe that the coefficients in Eq. (22) depend on (P,T) most sensitively through the fact that $c_p\sim\Delta T^{-\gamma}$ along the critical isochore, where $\Delta T=(T-T_c)/T_c$ and $\gamma=1.24$. Thus, making the approximations $(\partial T/\partial P)_\rho=T_c/5.92P_c$, $T^{(a)}=T^{(i)}=T_c$, and $c_v/c_p=0$, we find that

$$\frac{\partial T^{(a)}}{\partial z}=\rho\frac{\partial T^{(a)}}{\partial z'}\approx-\frac{\rho_c g T_c}{5.92P_c}\left[1-\left[\frac{\Delta T^{(i)}}{\Delta T^{(a)}}\right]^{-\gamma}\right]. \tag{23}$$

For the quench from 20 to 10 mK above T_c, Eq. (23) yields the value $\partial T^{(a)}/\partial z\approx-0.5$ mK/cm, which compares favorably with the slope observed in Fig. 2 (T_c,P_c, and ρ_c values are listed in Table I).

It is striking that the temperature gradient generated in this way is *negative*, i.e., temperature decreases with increasing height, as in Fig. 2. This naturally causes one to consider whether the one-dimensional flow might become unstable and develop into multidimensional, gravity-driven convective flows. A fundamental criterion for the mechanical stability of an inviscid, compressible fluid in mechanical equilibrium is that if an element of fluid rises adiabatically, it will remain denser than the fluid it displaces. As discussed by Landau and Lifshitz [23], the ensuing condition for the absence of convection is that the *entropy increases with height*, i.e.,

$$\frac{\partial s}{\partial z}>0. \tag{24}$$

(This presumes that the fluid expands on heating at constant pressure, i.e., $\alpha_p>0$.) It is evident from the discussion above that this condition remains true in the bulk of the fluid as long as processes proceed adiabatically.

Indeed, a small negative temperature gradient is permitted. This point has been previously discussed by several authors, e.g., Jeffreys [30], Gitterman [31], and Moldover *et al.* [14]. (Also see Sec. IV below.) Using Eq. (21), the condition from Eq. (24) is equivalent to

$$-\frac{\partial T}{\partial z}<\rho g\left[1-\frac{c_v}{c_p}\right]\left[\frac{\partial T}{\partial P}\right]_\rho. \tag{25}$$

The quantity on the right-hand side corresponds to a critical temperature gradient of about -1 mK/cm for near-critical xenon. It corresponds to the gradient generated in a fluid starting at equilibrium in zero gravity, when the fluid is accelerated adiabatically (as if gravity is switched on rapidly). The gradient generated by our adiabatic quench does not exceed this, so the bulk of the fluid remains mechanically stable against convection.

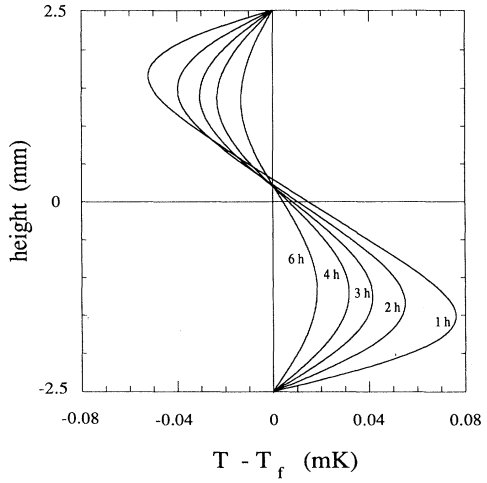

FIG. 6. Temperature profiles are shown along the height of the one-dimensional sample of xenon under gravity in the later stage of equilibration following a temperature quench from $T_i-T_c=20$ mK to $T_f-T_c=10$ mK. Each profile is labeled by the time in hours following the quench.

In Fig. 6 we show temperature profiles up to 6 h after the quench. We notice that the linear profile observed in the early stage disappears. Both the maximum and the minimum of the temperature profile in Fig. 6 tend to

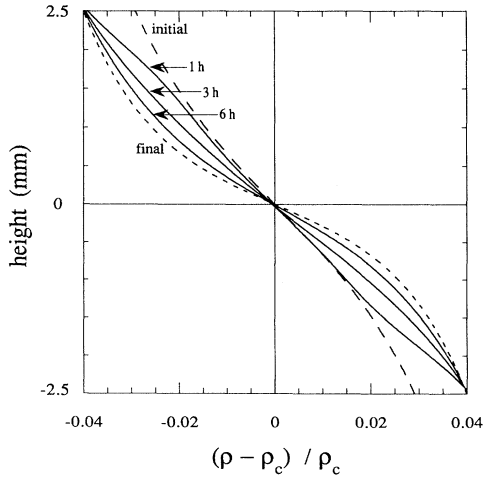

FIG. 7. Density profiles, in reduced units $(\rho-\rho_c)/\rho_c$, are shown along the height of a one-dimensional sample of xenon under gravity in the later stage of equilibration following a temperature quench from $T_i-T_c=20$ mK to $T_f-T_c=10$ mK. Each profile is labeled by the time in hours following the quench.

move inward to the center as time progresses. It is evident that this is due to diffusion and within a couple of hours, the magnitude of the temperature gradient near the boundaries has decreased to become comparable to that near the center.

In Fig. 7 we plot the density profile corresponding to the temperature profile in Fig. 6. The density profile remains close to symmetric around the center. Notice that the initial, larger density changes, which occurred early on at the boundaries (see Fig. 3), have disappeared within 1 h after the application of the quench.

A more interesting plot is the relative changes of the density at different heights. For this purpose we plot in Fig. 8 the distance of density from equilibrium as a function of time, for $h=\pm 2$ and ± 0.5 mm. Here $h=z'L/M$ and for convenience we regard h as height, making the approximation that density is constant. The reference $h=0$ corresponds to the center of the slab. In order to reduce the computational time and extend our calculations to later times ($t>36$ h), we set $\delta t'=0.2$ s, but we use the same number of segments ($N=400$).

As can be noticed in the semilogarithmic plot, it seems that the density equilibration is exponential for $t>5$ h, approximately. One expects a single fundamental mode to dominate the late stages of equilibration, with the same exponential decay rate at every height. But surprisingly, the decay rates measured from Fig. 8 distinctly appear to vary with height, in no obvious systematic way.

To examine this apparent height dependence, we plot in Fig. 9 a calculated decay rate as a function of time for $h=\pm 2$ and ± 0.5 mm. Specifically, we plot a smoothed value of

$$\alpha=-\left[\frac{1}{\Delta t'}\right]\ln\left[\frac{\rho_{n+2}-\rho_{n+1}}{\rho_{n+1}-\rho_n}\right], \tag{26}$$

as a function of time t_n'. Here ρ_n is the density calculated at time t_n' at a fixed height h. $\Delta t'=t_{n+1}'-t_n'$ is a fixed

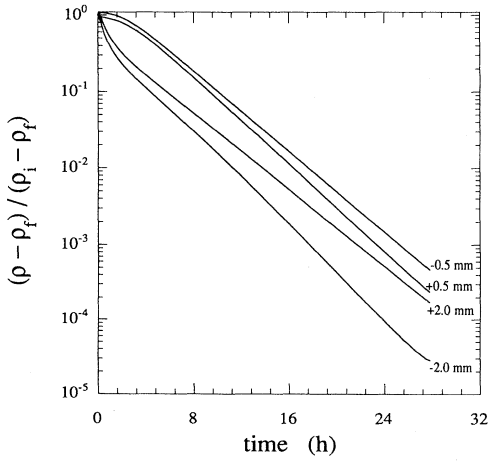

FIG. 8. The density, scaled by its initial value ρ_i and its final value ρ_f, is shown as a function of time following a temperature quench from $T_i-T_c=20$ mK to $T_f-T_c=10$ mK applied at a 5-mm-long xenon sample. Each curve is labeled by the distance measured in mm from the middle of the sample.

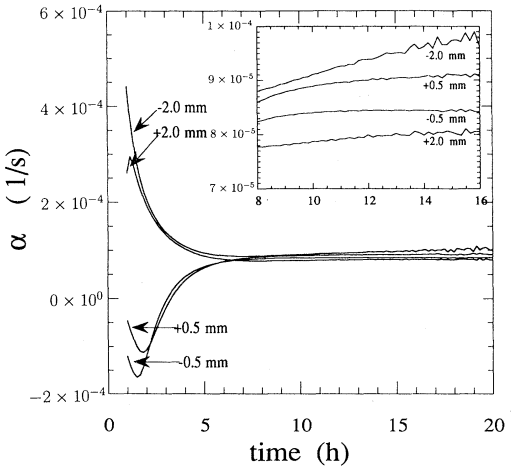

FIG. 9. The value of α (see text for definition) is shown as a function of time following the quench for different heights chosen in Fig. 8. The inset shows the details α in the intermediate regime.

time interval, which can be as small as the time step $\delta t'$. The formulas for α above is based on the supposition that $\rho=\rho_\infty+Ce^{-\alpha t}$, where ρ_∞, C, and α are unknown. The smoothing procedure used in Fig. 9 is simply to average $m=9$ successive values of α from Eq. (26), which is equivalent to replacing the numerator in the logarithm by $\rho_{m+n+1}-\rho_{m+n}$ and $\Delta t'$ and $m\Delta t'$.

From Fig. 9, it appears that α becomes close to constant in time after about 7 h, indicating pure exponential decay. However, it is apparent from the inset in Fig. 9 that α tends to vary slightly but distinctly with height, making it difficult to assert that one single fundamental mode comes to dominate the equilibration process in the first 24 h.

Despite this difficulty, we might compare the effective decay time $\tau_g=1/\alpha$ for $t>7$ h with the decay time $\tau_0=5.74$ h derived for the zero-gravity case corresponding to the same final temperature [1,4]. We find that τ_g varies between 2.82 and 3.45 h. Hence it appears that gravity tends to reduce the equilibration time. At $T_f=T_c+10$ mK, τ_g is about a factor of 2 smaller than τ_0.

IV. DISCUSSION AND REMARKS

The key to understanding the different time scales involved during relaxation processes in critical fluids is understanding the fluid's sensitivity to the various mechanisms driving the dynamics. In the temperature quench experiment that we have modeled, early adiabatic processes act rapidly to accomplish most of the temperature changes (in seconds), but induce only small density changes in the interior of the fluid. The importance of the adiabatic mechanism is in the strong coupling that it creates between temperature changes occurring at the fluid boundaries and the temperature response in the interior of the fluid [1–3,32]. It is evident that this coupling is still strong even when gravity is present (see Figs. 2 and 4). On the other hand, most of the rearrangement of the gravity-induced density profile is a nonadiabatic process,

driven by the much slower process of heat diffusion associated with tiny residual temperature variations. Therefore, the equilibration time for density variations is of the order of the diffusion time (hours).

The results in the present paper may help in interpreting equilibration times in critical fluids as measured by various experiments under similar boundary conditions, assuming that convective flow may be neglected. In general, we can distinguish two different groups of experiments: (i) those that probe directly the temperature changes and (ii) those that probe the density variations. Examples of the first group are C_v experiments, where short response times in one-phase systems were observed, corresponding to the fast adiabatic temperature responses [8,13,34,35]. For the second group, we can identify interferometric techniques, capacitance-measurements methods, and direct visual observations [12,36–39].

For $T > T_c$, C_v measurements taken on ^{3}He by Dahl and Moldover [8] near the critical point yielded upper bounds on equilibration times somewhere under 6 s. Similarly, Brown and Meyer [34] were unable in their early work to draw any information about the thermal relaxation time from their C_v measurement taken on ^{3}He in one phase. These observations are consistent with the mechanism of fast adiabatic temperature responses. Nitsche and Straub [9,13] confirmed this short time in an experiment performed in a TEXUS sounding rocket. They compared the temperature at the boundary with that at the center of a sample of SF_6 heated continuously from $T_c-0.4$ to $T_c+0.4$ K. They found that the temperature at the center of the fluid followed the temperature at the boundary regardless of the presence of gravity.

Recently, we have described a technique based on fluid transmission that can probe the fast temperature changes in critical xenon [5]. We used the fluid turbidity as a sensitive probe to monitor the temperature response to small heat pulses applied at the boundaries. We found very short response times, limited only by the container's glass wall separating the heater from the fluid.

In contrast, Greer [36] observed long relaxation times in her capacitance measurements taken on chlorine near the critical point ($T > T_c$). These long times are related to the density dynamics that are responsible for the changes in the capacitance. Since these measurements involve only overall density changes, it is not possible to derive much information about the local density changes during the stratification of the fluid in gravity. Similarly, Straub [12] recorded long relaxation times in his study of the dynamics of the gravity-induced density profile of N_2O (at $T = T_c + 25$ mK). In his experiment, the fast expansion and compression of the fluid during his measurements represent different boundary and initial conditions from those applied so far in our calculations. Nevertheless, his measurements show that perturbations of the density require a long time to relax even if the temperature returns quickly near its initial equilibration temperature. Unfortunately, we have not found any reported measurements of relaxation times taken by interferometric techniques, which are extensively used to study various properties of a fluid near its liquid-vapor critical point. Actually, some of these techniques take advantage of the gravity-induced density gradient in the fluid to derive, for example, the equation of state of the critical fluid [37–39]. Therefore, they are well suited to provide more information on the density of dynamics.

While we have emphasized the contrast between the fast temperature response and slow density changes in the problem we have addressed, different behaviors can be anticipated depending on the particular boundary conditions applied to the fluid and the proximity to the critical point. For example, Behringer, Onuki, and Meyer [10] reanalyzed earlier measurements of thermal relaxation times taken on ^{3}He near the critical point after including the adiabatic term in the thermal diffusion equation, without gravity. Interestingly, they compared two different sets of data—data derived from conductivity measurements [33] and data derived from C_v measurements [34] (calorimetiric)—which are taken under different boundary and initial conditions. In the conductivity measurements (for which some care had been taken to suppress convection), the experimental design permitted the measurement of thermal diffusion times through direct measurement of temperature differences. Agreement of theory with experiment was good [10], but degraded approaching the critical point, presumably due to the increased stratification caused by gravity. The equations derived here should be better adapted for including not only the adiabatic mechanism but also the effect of gravity.

For a correct interpretation of equilibration rate measurements, care should be taken to identify the regime in which the measurements are collected. For the example studied in this paper, our computations suggest that the adiabatic mechanism is effective just after the application of the temperature quench. A purely diffusive mode dominated by a single exponential will appear only after many hours. Our finding of a long, transient, intermediate regime (more than 24 h), in which the density variations near the top and bottom of the cell apparently exhibit exponential decay with different effective relaxation times, appears to corroborate observations of a similar phenomenon made by Zhong and Meyer [19–21]. Figure 10 specifically addresses this point. In a semilogarithmic

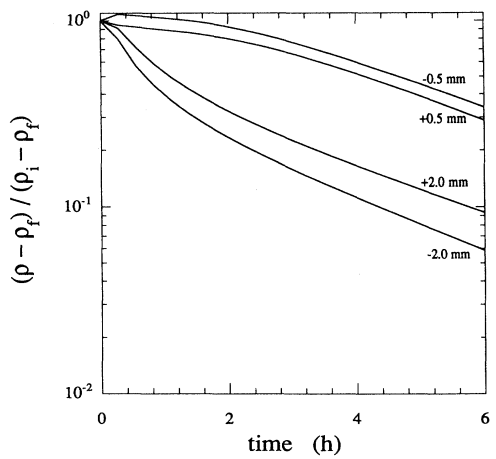

FIG. 10. Details of the first 6 h of Fig. 8.

plot, linear sections of the density equilibration curves strongly suggest an exponential behavior. However, the differing effective decay times indicate that the late-stage single-mode diffusive regime has not yet been reached (see Fig. 9). It may turn out that many experimental measurements fall in this intermediate regime and an interpretation of the data as being in the diffusive regime is erroneous. This clarification is important, as discrepancies may arise when comparing measured values with values calculated based on a single-mode analysis.

It would be interesting to derive a simple, explicit expression that gives the duration of this intermediate regime. For the zero-gravity case, Ferrell and co-workers showed that the adiabatic regime has a nonexponential, algebraic behavior that extends in time up to $t=\Gamma^2 t_1$ before late-stage diffusion dominates the equilibration [1,4]. Here we have $t_1=L^2/4D(\Gamma-1)^2$, $D=\lambda/\rho_c c_p$, and $\Gamma=c_p/c_v$. At $T_f=T_c+10$ mK and $\langle\rho\rangle=\rho_c$ (our example), we calculate $\Gamma^2 t_1=2.04\times10^5$ s. This is about 10 times longer than the period up to the onset of our intermediate regime, estimated from our computations (about 2.5×10^4 s; see Fig. 9). This suggests that, under gravity, diffusion takes over the equilibration sooner than in the zero-gravity situation.

In this present paper, we have focused on the one-phase region, but some of our results may be pertinent for understanding the dynamics of a two-phase system ($T<T_c$) when an interface appears. In a zero-gravity environment, one expects the liquid density ρ_L to approach the vapor density ρ_v as T_c is approached: $(\rho_L-\rho_v)\sim(T-T_c)^\beta$. In an earthbound experiment, however, gravity acts to substantially increase the equilibrium density gradient very near T_c. This should complicate data analysis of density relaxation taken in two-phase systems with gravity. The relaxation times observed will be subject to the same effects calculated here for one-phase systems, namely, large density variations relax very slowly and reduce the effectiveness of the adiabatic mechanism in accelerating the approach to equilibrium.

An interesting result obtained in the present calculations is the appearance of a small, almost linear temperature gradient at the beginning of the thermal equilibration process. This temperature gradient is absolutely necessary to sustain the slow changes in the density profile. The fluid appears to be in a state referred to sometimes as a long-lived nonequilibrium state [5,40]. In such a state, the critical fluid can have quite uniform density along its height. For example, such a situation can be experimentally produced by thoroughly stirring the fluid with convection [5,40]. In [40], Cannell noticed that his light-scattering measurements taken on a sample of SF_6 gave the same results (within experimental errors) whether the fluid was in the nonequilibrium state or was allowed to reach thermal equilibrium. This indicates that the fluid temperature in the long-lived nonequilibrium state is very close to the final equilibrium temperature, a situation similar to what we have seen in the calculations above (see Figs. 2 and 5). We have used a similar long-lived nonequilibrium state in our heat pulse experiment [5] to enhance the amplitude of the dynamic response, as more fluid has density closer to ρ_c.

Strikingly, the temperature gradient that is generated in the bulk of fluid early in our calculation is negative, but this is not expected to lead to the generation of convective, multidimensional flows. The reason is that the fluid's compressibility stabilizes the stratification. As discussed by a number of authors, notably Gitterman [31], and Jeffreys [30] much earlier, the appropriate Rayleigh number for determining the onset of convection in a compressible, viscous fluid involves not the temperature gradient directly, but rather its *excess* over the "adiabatic temperature gradient," which makes the entropy gradient zero [corresponding to the right-hand side of Eq. (25)]. As our calculations have suggested, this gives the experimenter some leeway in designing experiments that avoid gravity-driven convective flows.

The system of equations (14)–(16) are an improvement of the one-dimensional version of the equations derived in [2,22]. They include not only the adiabatic effect but also fluid motion due to expansion and contraction. As such, the model allows for the density gradients that occur in the final equilibrium state in a gravitational field. It will be of interest to investigate systematically not only how the system enters the late diffusive regime dominated by the fundamental mode but how all the modes develop during the equilibration. The present results do begin to provide, however, insight into the dynamics of stratification in one phase for a highly compressible, critical fluid under the influence of gravity. But we emphasize again that the system of equations (14)–(16) does not account for multidimensional flows, which are a strong possibility in many practical, three-dimensional situations. It is not yet clear how three-dimensional effects alter the overall dynamics under gravity, in general.

ACKNOWLEDGMENTS

The authors would like to thank J. N. Shaumeyer and J. V. Sengers for fruitful discussions. We also thank H. Meyer and F. Zhong for their comments and criticism of the first manuscript. This research is supported by NASA Contract No. NAS3-25370 and NSF Grant No. DMS92-01869.

APPENDIX A

In order to see how the system of equations (3), (5), and (6) can be appropriately reduced, we nondimensionalize and scale the variables in a manner appropriate to a typical experiment as follows. The critical density, pressure, and temperature are denoted ρ_c, P_c, and T_c, respectively. Let z_0 be a characteristic length, t_0 a characteristic time, and $u_0=z_0/t_0$. Let c_0 be a characteristic heat capacity and λ_0 a characteristic thermal conductivity. Let $g_0=z_0/t_0^2$ and introduce the following nondimensional variables and constants (nondimensional quantities are indicated by an asterisk):

$$\rho=\rho_c\rho^*,\quad P=P_c(1+P_0P^*),\quad T=T_c(1+T_0T^*)\,, \tag{A1}$$

$$z=z_0z^*,\quad t=t_0t^*,\quad u=u_0u^*\,, \tag{A2}$$

$$c_v = c_0 c_v^*, \quad c_p = c_0 c_p^*, \quad \lambda = \lambda_0 \lambda^*, \quad g = g_0 g^* , \tag{A3}$$

$$\kappa_T^* = \frac{1}{\rho^*}\left[\frac{\partial \rho^*}{\partial P^*}\right]_{T^*}, \quad \alpha_P^* = -\frac{1}{\rho^*}\left[\frac{\partial \rho^*}{\partial T^*}\right]_{P^*} . \tag{A4}$$

Above, P_0 and T_0 are scales characterizing the nondimensional deviation of the pressure and temperature from critical. The nondimensional equations corresponding to Eqs. (3), (5), and (6) are

$$\kappa_T^* \frac{DP^*}{Dt^*} - \alpha_P^* \frac{DT^*}{Dt^*} + \frac{\partial u^*}{\partial z^*} = 0 , \tag{A5}$$

$$M^2 \frac{Du^*}{Dt^*} + \frac{1}{\rho^*}\frac{\partial P^*}{\partial z^*} = -M^2 g^* , \tag{A6}$$

$$\frac{DT^*}{Dt^*} - \left[1 - \frac{c_v^*}{c_p^*}\right]\left[\frac{\partial T^*}{\partial P^*}\right]_{\rho^*}\frac{DP^*}{Dt^*} = \frac{D^*}{\rho^* c_p^*}\frac{\partial}{\partial z^*}\left[\lambda^* \frac{\partial T^*}{\partial z^*}\right] . \tag{A7}$$

Here the dimensionless groups M^2 and D^* are defined by

$$M^2 = \frac{\rho_c u_0^2}{P_c P_0}, \quad D^* = \frac{\lambda_0}{\rho_c c_0}\frac{t_0}{z_0^2} . \tag{A8}$$

D^* is a nondimensional diffusivity and M resembles a Mach number [24].

A typical flow regime in which we are interested is the one considered in [2]. The fluid is xenon, with critical parameters $\rho_c = 1.11\times10^3$ kg/m^3, $P_c = 5.84\times10^6$ Pa, and $T_c = 289.72$ K. Gravity effects tend to be important within 30 mK of T_c. For this temperature range, it is appropriate to take $P_0 = 6\times10^{-4}$, $T_0 = 10^{-4}$, $c_0 = 3.3\times10^6$ J/K kg, and $\lambda_0 = 2.5\times10^{-1}$ J/s m K. For z_0 and t_0, we chose $z_0 = 10^{-3}$ m and $t_0 = 1$ s. These yield the following estimate for the dimensionless parameters: $D^* = 6\times10^{-5}$, $M^2 = 3\times10^{-7}$, $c_v^*/c_p^* = 1.8\times10^{-4}$, $g^* = 9.81\times10^3$, and $(\partial T^*/\partial P^*)_\rho^* \sim 1$.

In the systems of equations (A5)–(A7), one tries to choose the scales so that the dimensionless variables P^*, T^*, u^* and their derivatives are of the order of 1. The importance of each term in the dynamical equations is determined by the dimensionless prefactor preceding it. Our interest is in the density variation due to the pressure gradient caused by gravity and the effect of the heat diffusion to bring the system to equilibrium. The acceleration term $M^2 Du^*/Dt^*$ is by far the smallest term (about two orders of magnitude smaller than the next term). Furthermore, note the effect of considering longer time scales. As t_0 increases, M^2 decreases quadratically, D^* increases, and the group $M^2 G$ does not change. Thus, in the time range of interest to us in this paper, it seems justifiable to neglect the acceleration term and it is *only* this term that we have neglected (in addition to the effects of viscosity) to obtain a reduced system of equations.

APPENDIX B

In this appendix we describe how we convert the pressure and temperature (P,T) into their corresponding values of r and θ used in the restricted cubic model. In that model, the dimensionless temperature increment and pressure are expressed as

$$\Delta T^* = \frac{T - T_c}{T_c} = r(1 - b^2\theta^2) , \tag{B1}$$

$$P/P_c = P_a^*(T) + r^{\beta\delta}\theta(1-\theta^2) + r^{2-\alpha}ak\{\theta^2(1-\theta^2)(1+c\theta^2) - f(\theta)\} . \tag{B2}$$

Here $P_a^*(T)$ is an analytic function of temperature that represents the pressure along the critical isochore $(\rho = \rho_c)$. The rest is the nonclassical scaled part. In the pressure, the function $f(\theta)$ is expanded as a series in θ,

$$f(\theta) = f_0 + f_2\theta^2 + f_4\theta^4 + f_6\theta^6 + \cdots , \tag{B3}$$

where the coefficients f_0, f_2, f_4, and f_6 are listed in Table I. We take $P_a^*(T) = (1 + 5.92\Delta T^*)$ (see [27] and references therein).

For a given set of values (P_0, T_0), we wish to find the zero of the function $g(r,\theta)$ defined as

$$g(r,\theta) = P_0 - P_a^*(T) - r^{\beta\delta}a\theta(1-\theta^2) - r^{2-\alpha}ak\{\theta^2(1-\theta^2)(1+c\theta^2) - f(\theta)\} , \tag{B4}$$

with the condition that $\Delta T^* = (T_0 - T_c)/T_c = r(1 - b^2\theta^2)$ is fixed. For this purpose, we apply the Newton-Raphson numerical method. First, we express r in terms of θ via $r = \Delta T^*/(1 - b^2\theta^2)$ and substitute into the function $g(r,\theta)$, which becomes a function of θ only. Then, we find $g'(\theta)$, the derivative of $g(\theta)$ with respect to θ. Finally, we solve the equation $g(\theta) = 0$ using the iteration

$$\theta_{n+1} = \theta_n - g(\theta_n)/g'(\theta_n) .$$

To start the iteration, the initial θ value is set close to $1/b$.

[1] A. Onuki, H. Hong, and R. A. Ferrell, Phys. Rev. A **41**, 2256 (1990).

[2] H. Boukari, J. N Shaumeyer, M. E. Briggs, and R. W. Gammon, Phys. Rev. A **41**, 2260 (1990).

[3] B. Zappoli, D. Baily, Y. Garrabos, B. Le Neindre, P. Guenoun, and D. Beysens, Phys. Rev. A **41**, 2264 (1991).

[4] A. Onuki and R. A. Ferrell, Physica A **164**, 245 (1990); R. A. Ferrell and H. Hao, *ibid.* **197**, 23 (1993).

[5] H. Boukari, M. E. Briggs, J. N. Shaumeyer, and R. W. Gammon, Phys. Rev. Lett. **65**, 2654 (1990).

[6] H. Klein, G. Schmitz, and D. Woermann, Phys. Rev. A **43**, 4562 (1991).

[7] P. Guenoun, B. Khalil, D. Beysens, Y. Garrabos, F. Kammoun, B. Le Neindre, and B. Zappoli, Phys. Rev. E **47**, 1531 (1993).
[8] D. Dahl and M. R. Moldover, Phys. Rev. A **6**, 1915 (1972).
[9] K. Nitsche and J. Straub, in *Proceedings of the Sixth European Symposium on Material Sciences under Microgravity Conditions, Bordeaux, 1986* (European Space Agency, Paris, 1987), Vol. SP-256, p. 109.
[10] R. P. Behringer, A. Onuki, and H. Meyer, J. Low. Temp. Phys. **81**, 71 (1990).
[11] H. Klein and B. Feuerbacher, Phys. Lett. A **123**, 183 (1987).
[12] J. Straub, Doctoral dissertation, Technische Universität, München, 1965 (unpublished); results presented by E. H. Schmidt, in *Critical Phenomena,* edited by M. S. Green and J. V. Sengers, Proceedings of the Conference on Phenomena in the Neighborhood of Critical Points (National Bureau of Standards, Washington, DC, 1966), p. 13.
[13] J. Straub and K. Nitsche, in *Proceedings of the 11th Symposium of Thermophysical Properties, Boulder, 1991* [Fluid Phase Equil. **88**, 183 (1993)].
[14] M. R. Moldover, J. V. Sengers, R. W. Gammon, and R. J. Hocken, Rev. Mod. Phys. **51**, 79 (1979).
[15] P. C. Hohenberg and M. Barmatz, Phys. Rev. A **6**, 289 (1972).
[16] A. L. Sengers, R. Hocken, and J. V. Sengers, Phys. Today **30**, (12) (1977), and references therein.
[17] M. Sh. Gitterman and V. A. Shteinberg, Teplofiz. Vys. Temp. **8**, 799 (1970) [High Temp. **8**, 754 (1971)].
[18] R. F. Berg, Phys. Rev. E **48**, 1799 (1993).
[19] F. Zhong and H. Meyer, NASA Document No. JPL D-11775, 1994 (unpublished), p. 62.
[20] F. Zhong and H. Meyer, NASA Document No. JPL D-11755 (Ref. [19]), p. 73.
[21] F. Zhong and H. Meyer, in *Fluid Mechanics Phenomena in Microgravity,* edited by D. A. Signier, R. L. Thompson, and L. M. Trefethen, special issue of J. Am. Soc. Mech. Eng. **174**, 139 (1993).
[22] H. Boukari, Ph.D. thesis, University of Maryland, 1992 (unpublished).
[23] L. D. Landau and E. M. Lifshitz, *Fluid Mechanics,* 2nd ed. (Pergamon, Oxford, 1987).
[24] A. Majda and J. Sethian, Combust. Sci. Tech. **42**, 185 (1985).
[25] A. Majda, *Compressible Fluid Flow and Systems of Conservation Laws in Several Space Variables,* Applied Mathematical Sciences Vol. 53 (Springer, New York, 1984).
[26] R. G. Rehm and H. R. Baum, J. Res. Natl. Bur. Stand. **83**, 297 (1973).
[27] H. L. Swinney and D. L. Henry, Phys. Rev. A **8**, 2586 (1973), and references therein.
[28] J. Sengers, Int. J. Thermophys. **6**, 203 (1985).
[29] R. F. Berg and M. R. Moldover, J. Chem. Phys. **93**, 1926 (1990).
[30] H. Jeffreys, Proc. Cambridge Philos. Soc. **26**, 170 (1930).
[31] M. Gitterman, Rev. Mod. Phys. **50**, 85 (1978).
[32] B. Zappoli, Phys. Fluids A **4**, 1040 (1992).
[33] C. E. Pittman, L. H. Cohen, and H. Meyer, J. Low Temp. Phys. **46**, 115 (1982).
[34] G. R. Brown and H. Meyer, Phys. Rev. A **6**, 364 (1972).
[35] J. A. Lipa, C. Edwards, and M. J. Buckingham, Phys. Rev. A **15**, 778 (1977).
[36] S. Greer, Phys. Rev. A **31**, 3240 (1985).
[37] D. A. Balzarini, Can. J. Phys. **50**, 2194 (1972).
[38] W. T. Estler, R. Hocken, T. Charlton, and L. R. Wilcox, Phys. Rev. A **12**, 2118 (1975).
[39] M. R. Moldover, *Phase Transitions: Cargese 1980,* edited by M. Levy, J. C. Le Guillou, and J. Z. Justin (Plenum, New York, 1980).
[40] D. S. Cannell, Phys. Rev. A **12**, 225 (1975).